Title

Pyrolysis of Two Perfluoroalkanesulfonates (PFSAs) and PFSA-Laden Granular Activated Carbon (GAC): Decomposition Mechanisms and the Role of GAC

Journal

Environmental Science and Technology, 58(49)

ISSN

0013-936X

Authors

Wang, Junli

Chen, Kunpeng

Jin, Bosen

et al.

Publication Date

2024-12-10

DOI

10.1021/acs.est.4c06805

Peer reviewed

Environmental Science & Technology

pubs.acs.org/est

Article

Pyrolysis of Two Perfluoroalkanesulfonates (PFSAs) and PFSA-Laden Granular Activated Carbon (GAC): Decomposition Mechanisms and the Role of GAC

Junli Wang, Kunpeng Chen, Bosen Jin, Wonsik Woo, Michael Lum, Alexa Canchola, Yiwen Zhu, Yujie Men, Jinyong Liu, and Ying-Hsuan Lin*

Cite This: *Environ. Sci. Technol.* 2024, 58, 21850−21860

Read Online

ACCESS | Metrics & More | Article Recommendations | Supporting Information

ABSTRACT: Thermal treatment of perfluoroalkyl and polyfluoroalkyl substances (PFASs) presents a promising opportunity to halt the PFAS cycle. However, how co-occurring materials such as granular activated carbon (GAC) influence thermal decomposition products of PFASs, and underlying mechanisms remain unclear. We studied the pyrolysis of two potassium salts of perfluoroalkanesulfonates (PFSAs, $C_nF_{2n+1}SO_3K$), perfluorobutanesulfonate (PFBS-K), and perfluorooctanesulfonate (PFOS-K), with or without GAC. PFBS-K is more stable than PFOS-K for pure standards, but when it is adsorbed onto GAC, its thermal stabilities and decomposition behaviors are similar. Temperatures and heating rates can significantly influence the decomposition mechanisms and products for pure standards, while these effects are less pronounced when PFSAs are adsorbed onto GAC. We further studied the underlying decomposition mechanisms. Pure standards of $C_nF_{2n+1}SO_3K$ can decompose directly in their condense phase by reactions: $F(CF_2)_nSO_3K \rightarrow F(CF_2)_{n-2}CF{=}CF_2 + KFSO_3$ or $F(CF_2)_nSO_3K \rightarrow F(CF_2)_n^- + K^+ + SO_3$. GAC appears to facilitate breakage of the C−S bond to release SO_2 at temperatures as low as 280 °C. GAC promotes fluorine mineralization through functional reactive sites. SiO_2 is particularly important for the surface-mediated mineralization of PFASs into SiF_4. These findings offer valuable insights into optimizing thermal treatment strategies for PFAS-contaminated waste.

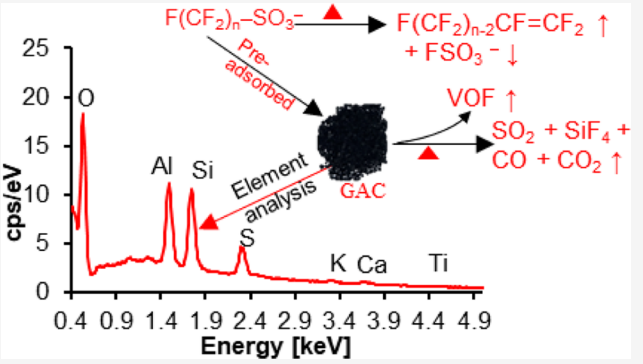

KEYWORDS: *PFBS, PFOS, PFAS, sorbent treatment, pyrolysis, surface-mediated decomposition, functional reactive site, silica*

1. INTRODUCTION

Per- and polyfluoroalkyl substances (PFASs) are persistent man-made chemicals that have been widely detected in natural waters and industrial wastes,[1−4] and have raised substantial concern for ecosystems and human health.[5−9] When the source of drinking water is contaminated, PFASs cannot be efficiently removed in conventional water treatment plants.[10,11] A few technologies have emerged to degrade PFASs for water treatment, such as electrochemical degradation,[12,13] ultraviolet/sulfite/iodine,[14−18] and plasma-based degradation;[19−21] however, most of them have only been tested in laboratory settings or still in the effort of scaling up.[22,23] PFAS adsorption from water by granular activated carbon (GAC) or ion exchange (IX) resins is one of the most established approach that can be deployed in full-scale because of its economic effects, compatibility, and regeneration potential.[24−26]

When PFASs are concentrated on GAC, the spent GAC requires further treatment to prevent the PFASs from reentering the environment.[27,28] Thermal reactivation is a well-established process to treat spent GAC,[29−31] and most PFASs can be removed in the thermal treatment.[29,32−34] The reactivation involves two stages: (1) a pyrolytic process to remove and destroy adsorbates in an inert atmosphere; and (2) an oxidative process to reactivate the GAC by gasification reactions in steam or carbon dioxide atmosphere around 800 °C.[30,35] Adsorbed PFASs can be thoroughly removed (>99%) and partial mineralization of fluorine (30−72%) can be obtained in the pyrolytic stage.[36,37] Perfluoroalkanesulfonates (PFSAs) require higher temperatures (400 °C) than perfluoroalkyl carboxylic acids (PFCAs) and emerging carboxylate structures such as GenX.[32,34] Although PFSAs are one of the most common and thermally resistant PFAS categories found in the environment, current mechanistic

Received: July 5, 2024
Revised: October 31, 2024
Accepted: November 18, 2024
Published: November 26, 2024

https://doi.org/10.1021/acs.est.4c06805
Environ. Sci. Technol. 2024, 58, 21850−21860

understanding about the thermal treatment of PFSAs is limited.

Prior studies of the thermal decomposition of PFSAs focused on the acidic form ($C_nF_{2n+1}SO_3H$) as pure standards at specific temperatures. For example, pyrolysis of perfluorooctanesulfonic acid (PFOS-H) pure standards has been reported to release HF, SO_2, COF_2, C_2F_4, and perfluorooctanoyl fluoride ($C_7F_{15}COF$) as major products in computational and experimental studies.[38−41] However, earlier understandings from $C_nF_{2n+1}SO_3H$ may not be directly applicable to the anions ($C_nF_{2n+1}SO_3^-$) existing in the environment due to the dissociation caused by pH, considering the low pK_a (typically <2) of PFSAs.[42] In addition, GAC could alter the PFAS thermal decomposition mechanisms and enhance the mineralization rates in the thermal treatment processes,[33,37] yet the underlying mechanisms have not been fully understood. Furthermore, thermal treatment of GAC involve the ramp heating step, but the thermal behaviors of PFASs during ramp heating process have not been studied.[27,30] Finally, there has been little experimental research on the thermal decomposition of shorter-chain PFSAs, such as PFBS, leaving a significant knowledge gap regarding the influence of the perfluorocarbon chain on thermal decomposition mechanisms.

The objectives of this study are to investigate: (1) the thermal decomposition products and mechanisms of deprotonated PFSAs using a combination of experimental and computational approaches; (2) the thermal behaviors of pure PFSA standards and PFSA-laden GAC to understand the role of GAC in PFSA thermal decomposition and mineralization; (3) the influence of temperature and heating methods (e.g., ramp heating or isothermal conditions used in GAC regeneration) on product formation; and (4) the influence of perfluorocarbon chain length on PFSA thermal decomposition. The results of this study contribute to an improved understanding of thermal treatment for PFAS remediation, which can aid in the development of more cost-effective and sustainable strategies for PFAS waste management.

2. MATERIALS AND METHODS

2.1. Chemicals. Four PFASs were used in this study: perfluorobutanesulfonic acid (PFBS-H, 98%, TCI America), potassium perfluorobutanesulfonate (PFBS-K, 98%, TCI America), perfluorooctanesulfonic acid (PFOS-H, 95%, Matrix Scientific), and potassium perfluorooctanesulfonate (PFOS-K, 98%, Matrix Scientific). Potassium fluorosulfate ($KFSO_3$, 99.5%) was purchased from Thermo Scientific. FILTRASORB 400 GAC (Calgon Carbon Corporation, Pittsburgh, PA) was used in this study for its high PFAS sorption capability and common use in commercial systems.[27,43−45] PFSA-laden GAC samples were prepared by bench adsorption experiments. Detailed chemical information and preparations of GAC samples can be found Supporting Informationand in Table S1.

2.2. Experimental Methods. Samples were ramp heated or heated in isothermal conditions. Ramp heating process specifically means that the furnace and sample are heated simultaneously from room temperature with a rate of 10 °C min^{-1}, while heating in isothermal conditions means a furnace is preheated and maintained to 500 or 600 °C before and after samples are introduced in this study. Ramp heating of ∼10 mg pure PFSAs standards or ∼30 mg PFSA-laden GAC in aluminum crucibles was conducted with a simultaneous thermal analyzer (STA, NETZSCH STA 449 F1 Jupiter) equipped with a silicon carbide furnace at Iowa State University. The temperatures increased from 40 to 1100 °C, with a rate of 10 °C min^{-1}. Thermogravimetry (TGA) and differential scanning calorimetry (DSC) data were acquired simultaneously. The STA was coupled with a quadrupole mass spectrometer (NETZSCH Aeolos QMS 403 D) and a Fourier-transform infrared (FTIR, Bruker ALPHA II) spectrometer to monitor evolved gaseous products that were correlated with TGA and DSC signals. In the following sections, STA-MS/FTIR refers to the simultaneous thermal analysis of TGA/DSC and analysis of gaseous products with MS/FTIR. Additional experiments were conducted to confirm the reproducibility of STA-MS/FTIR analysis (SI). An MTI tube furnace (OTF-1200X) equipped with a ceramic tube was also used for additional ramp heating experiments to exclude the interference of silicon. The detailed parameters of the thermal treatment instrument can be found in Figure S1.

To aid in the interpretation of the STA-MS/FTIR results, we conducted pyrolysis experiments under isothermal conditions (preheated at 500 and 600 °C) using an electric tube furnace modified from a Shimadzu solid sample module (SSM-5000A). SSM-5000A was fitted with a quartz tube or stainless steel 316 tube, which was flowed by ultrahigh purity N_2 at a flow rate of 100 mL min^{-1}. An FTIR spectrometer (Nicolet Magna-IR 560) at a resolution of 2 cm^{-1} equipped with a 2 m optical-path gas cell was connected to the outflow of furnaces to monitor the evolved gases in real time. The system was purged by N_2 more than 1 h at 500 or 600 °C and monitored by FTIR to exclude the interferences of impurities or carryovers before pyrolysis experiments started. The experiments were conducted two to three times to confirm the findings. Gaseous products were identified through spectral comparison with standard references from published papers or databases.[46−50] The OMNIC software (Thermo Scientific) was used to perform FTIR spectra subtraction. Qualitative analysis for pyrolysis residuals was conducted with attenuated total reflectance FTIR (ATR-FTIR, ThermoFisher Scientific Nicolet iS50) and ultrahigh-resolution mass spectrometry (UHPLC-HRMS, Q Exactive Plus, Thermo Scientific). Details are provided in Supporting Information. The UHPLC-HRMS instrumental settings and product identification procedures have been published elsewhere.[51]

Scanning electron microscopy (SEM, TESCAN, Vega3 SBH) coupled with energy dispersive X-ray spectroscopy (EDS, Bruker, XFlash7T) was used to characterize the elemental composition of the GAC surfaces pre- and postpyrolysis experiments.

2.3. Calculation of Theoretical Potential Energy Profiles. Thermal degradation mechanisms of PFBS and PFOS were studied through quantum chemical calculations based on density functional theory (DFT) and transition state theory (TST). The influence of the crystal structures on the decomposition is not considered in this study. The suite of Gaussian 16 programs was used to optimize the geometries of reactants, products, intermediates, and transition states using the Boese and Martin's τ-dependent hybrid functional (BMK)[52] and 6−31+G(2d,p) basis set.[53] Frequency analysis was conducted by the same method, and the electronic energies were computed using double-hybrid functional DSD-PBEP86,[54] in combination with Grimme's third-generation empirical dispersion implemented by Becke-Johnson damping (D3BJ),[55] and the triple-ζ basis set def2-TZVP.[56] Intrinsic reaction coordinate calculations were carried out to verify the transition state connectivity.[57] Previous studies have demon-

https://doi.org/10.1021/acs.est.4c06805
Environ. Sci. Technol. 2024, 58, 21850−21860

strated that the calculated decomposition pathways using these functional and basis sets are satisfactory[41,58] and consistent with experimental results.[38−40,59] Instead of targeting the precise values of energy barriers, our computation can qualitatively point out feasible pathways during the thermal decomposition of PFSAs. When PFBS/PFOS were preadsorbed onto GAC, their decomposition pathways were primarily derived from experimental results rather than computation, given that the DFT calculations were performed intrinsically in vacuum without any interaction with surrounding environments.

3. RESULTS AND DISCUSSION

3.1. Pyrolysis of Pure PFBS-K and PFOS-K Standards.

3.1.1. Simultaneous Thermal Analysis and Gaseous Products in Ramp Heating. Pure standards of ∼10 mg PFBS-K/PFOS-K were heated from 40 to 1000 °C for STA-MS/FTIR analysis. The TGA and DSC curves, mass spectra, and FTIR at 488 °C of gaseous products are shown in Figure 1. The TGA curve of PFBS-K did not significantly change until

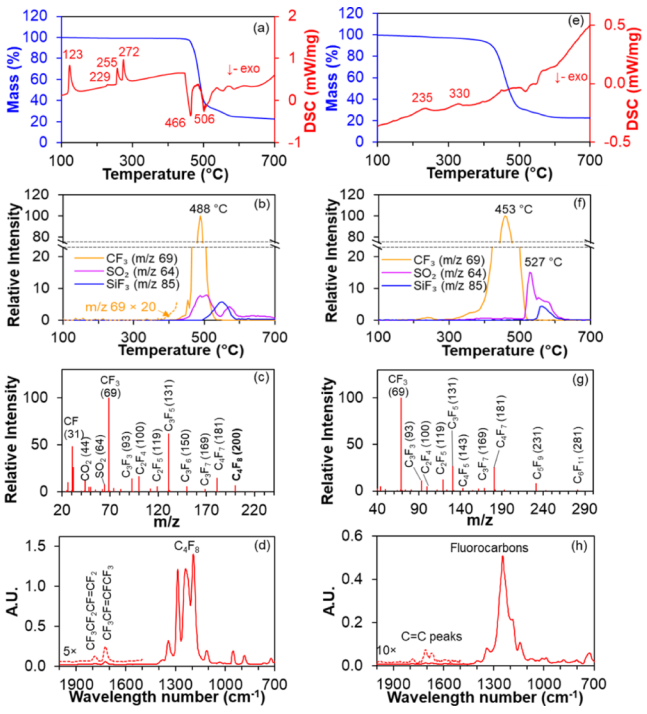

Figure 1. STA-MS/FTIR analysis of PFBS-K (a−d) and PFOS-K (e−h), respectively: (a) and (e) TGA/DSC curve, (b) and (f) formation trends of selected gaseous products represented by EI fragments, (c) and (g) mass spectrum of gaseous products at 488 °C EI (70 eV), and (d) and (h) FTIR spectrum (resolution, 4 cm^{-1}) of gaseous products at 488 °C for PFBS-K and 453 °C PFOS-K, respectively. Reference FTIR spectra of $CF_3CF_2CF{=}CF_2$ and $CF_3CF{=}CFCF_3$ can be found in published literature.[46,60] More mass spectra and FTIR spectra can be found in Figure S2 (PFBS-K) and Figure S5 (PFOS-K).

430 °C (98.92% mass left). However, PFBS-K started to yield organofluorine gases at temperatures as low as ∼380 °C, as indicated by the increase in the CF_3 (m/z 69) signal in gaseous products detected by MS (Figure 1b). Thus, PFBS-K can be considered thermally unstable above 380 °C.

The significant mass loss (61.45%) of PFBS-K between 448 °C (98.46% remaining) and 506 °C (37.01% remaining) indicates that thermal decomposition occurred in its condensed phase and decomposed into gaseous products before reaching the boiling point (transitioning into the gas phase). At this stage, the DSC curve shows a distinct exothermic peak at 466 °C, which further excludes the evaporation of PFBS-K because evaporation is an endothermic process. The observed mass loss can be attributed to the formation of gaseous products, such as organofluorine (represented by CF_3 m/z 69) and SO_2 (m/z 64), as shown in Figure 1b and1c. By comparing with reference FTIR spectra published in literature,[46,60] the products at 488 °C include $CF_3CF{=}CFCF_3$ (2-C_4F_8) and $CF_3CF_2CF{=}CF_2$ (1-C_4F_8) (Figure 1d). Additional FTIR and mass spectra obtained at various temperatures are shown in Figure S2. The identified products from FTIR spectra were further supported by MS. For example, all EI fragments of 1-C_4F_8 and 2-C_4F_8, such as m/z 200 ($C_4F_8^+$), m/z 181 ($C_4F_7^+$), and m/z 131 ($C_3F_5^+$) were detected and agreed well with the NIST references (Figure S3).

The second stage of mass loss, occurring between temperatures of 506 °C (37.01% remaining) and 588 °C (24.74% remaining), exhibits a decrease in rate compared to the initial stage. The DSC curve suggests that the second stage consisted of multiple processes, characterized by indistinguishable peaks between the temperature from 506 to 650 °C. The gaseous products detected by MS and FTIR (Figure S2) indicated the presence of SO_2F_2 (Figure S5), SiF_4, and SO_2 (Figure 1b). One possible explanation is that the second stage involves the further decomposition of residual products such as $KFSO_3$ (see Sections 3.1.2 and 3.2.2) from the first stage when temperatures increased. This is evidenced by the shift of the dominant gaseous products from organofluorine or olefins to inorganic gases such as SO_2 and SiF_4. SiF_4 is likely produced through the reaction of intermediates with SiC, which is the reactor material of the tube furnace. SiF_4 is frequently observed during the thermal decomposition of PFASs when silicon-based materials such as quartz and glass are present.,[49,61,62] Thus, the thermal decomposition of PFBS-K does not follow a single pathway but rather involves multiple pathways and processes.

The TGA curve of PFOS-K (Figure 1e) exhibits similarities to that of PFBS-K. The first stage of mass loss occurred between temperatures of 400 and 506 °C, resulting in the release of organofluorine gases, including olefins (Figure 1h). Both the FTIR spectrum (Figure 1h) and mass spectrum (Figure 1g) can demonstrate that the released gases were fluorocarbons. At 448 °C, two peaks at 1782.79 and 1709.78 cm^{-1} in FTIR spectra, corresponding to C═C bonds (Figure 1h), most likely represent formations of perfluoro-1-octene ($CF_3(CF_2)_5CF{=}CF_2$, 1-C_8F_{16}), and perfluoro-2-octene ($CF_3(CF_2)_4CF{=}CFCF_3$, 2-C_8F_{16}) (S4), similarly with decomposition of PFBS-K (Table 1). The second stage of mass loss occurred between 506 and 600 °C, releasing inorganic gases such as SO_2, SiF_4, and SO_2F_2 (Figure S4). At temperatures exceeding 500 °C, the primary gaseous products were SO_2 and SiF_4, while organofluorine products were no longer detected (Figure 1f). Similar trends of TGA curves and decomposition products (e.g., corresponding olefins, SO_2, SiF_4) imply that PFOS-K underwent similar decomposition processes as PFBS-K.

However, the thermal decomposition of PFOS-K also exhibits unique characteristics (Table 1). First, the onset of PFOS-K thermal decomposition occurs at lower temperatures (300 °C) compared to that of PFBS-K (380 °C). The DSC peaks at ∼330 °C (Figure 1e) and associated VOF detection

https://doi.org/10.1021/acs.est.4c06805
Environ. Sci. Technol. 2024, 58, 21850−21860

Table 1. Comparisons of the Thermal Behaviors of PFBS and PFOS at Different Conditions

Conditions	Similarities	Differences
PFBS-K vs PFOS-K	Trends of TGA curves; Decomposition pathways (reaction 1) and products (olefins, SO_2, SiF_4, C_2F_4, $KFSO_3$, SO_2F_2).	PFOS-K is less thermally stable; PFBS-K has multiple endothermic peaks before mass loss; Different decomposition mechanism to form SO_2; Pyrolysis of PFOS-K produced C_2F_6 at 600 °C.
GAC laden with PFBS vs PFOS	TGA curves; Exothermic reactions at ~448 °C; Thermal stabilities; Decomposition products (olefins, SO_2, SiF_4, C_2F_4).	PFOS yields longer perfluorocarbon chain products.
PFSA-K vs PFSA-laden GAC	Decomposition products (olefins, SO_2, SiF_4, C_2F_4).	GAC promotes pyrolysis of PFSAs to (1) yield more SO_2 but less VOF; (2) form SiF_4; (3) produce hydrofluorocarbons; (4) reduce their thermal stabilities; (5) change decomposition mechanisms and thermal behaviors.

(e.g., CF_3^+, m/z 69, Figure 1f) indicate the formation of gaseous products. In addition, the DSC curve for PFOS-K did not show any discernible exothermic peaks during the initial stage of mass loss. Furthermore, in contrast to PFBS-K, the pyrolysis of PFOS-K results in asynchronous formation peaks of VOF (e.g., CF_3^+ m/z 69) and SO_2 (m/z 64), with the later formation peak of SO_2 observed at 527 °C (Figure 1f). PFBS-K and PFOS-K belong to PFSAs with similar molecular structures, which were tested under the same conditions. Different thermal behaviors, including different thermal stabilities, DSC curves, and timings of produce gaseous products, were observed in ramp heating. One possible explanation is that crystal structures[63] caused by perfluorocarbon chain lengths (C4 vs C8) can influence thermal behaviors of potassium salts of PFSAs.

3.1.2. Product Analysis at 500 and 600 °C (Isothermal Conditions). During the ramping heating process, PFBS-K and PFOS-K were decomposed below 500 °C. However, the effects of the temperatures on the resulting decomposition products remain unclear, as the heating rate may alter the kinetic behavior and influence the pyrolysis process. We conducted additional research on the pyrolysis of PFBS-K and PFOS-K under isothermal conditions at 500 and 600 °C, respectively. FTIR was used to monitor the gaseous products, with the corresponding spectra presented in Figure 2. Based on the FTIR spectra, we identified a series of products: (1) at 500 °C, pure PFBS-K produced 1-C_4F_8 (C=C stretching at 1792.69 cm^{-1}), 2-C_4F_8 (C=C stretching at 1730.37 cm^{-1}), C_2F_4, SO_2, and some unknown compounds; (2) at 600 °C, the primary product of PFBS-K was $CF_3CF{=}CFCF_3$, with minor amounts of C_2F_4 and SO_2 also being produced. Similar products were also detected during the pyrolysis of PFOS-K: (1) at 500 °C, a C=C peak at 1792.08 cm^{-1} and a C=C peak at 1718.60 cm^{-1} (Figure 2c) suggested the formation of 1-C_8F_{16} and 2-C_8F_{16} (S4), respectively; (2) SO_2 and C_2F_4 were detected at 500 and 600 °C. The formations of 1-C_8F_{16} and 2-C_8F_{16} were also confirmed in another recent publication.[64] In addition, formations of hexafluoropropene (C_3F_6), perfluorobutane (C_4F_{10}), perfluoro-1-heptene(1-C_7F_{14}), perfluoro-1-hexene (1-C_6F_{12}), perfluoro-2-hexene (1-C_6F_{12}) in pyrolysis of PFOS-K were also reported.[64]

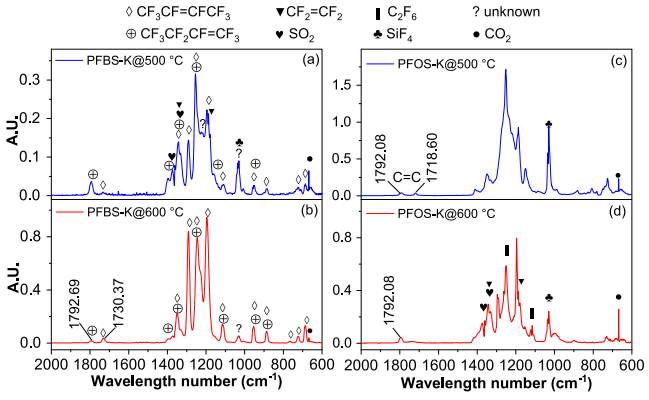

Figure 2. FTIR spectra (resolution, 2 cm^{-1}) of gaseous products in the pyrolysis of (a) PFBS-K at 500 °C, (b) PFBS-K at 600 °C, (c) PFOS-K at 500 °C, (d) PFOS-K at 600 °C. Reference FTIR spectra of $CF_3CF_2CF{=}CF_2$ and $CF_3CF{=}CFCF_3$ can be found in published literature.[46,60] Subtracted spectra from features attributable to C_2F_4 ($CF_2{=}CF_2$) and C_2F_6 can be found in Figures S6 and S7.

Notably, the decomposition products of PFOS-K can be significantly influenced by the temperature changes. New products such as C_2F_6 and some unknown perfluorocarbons were identified at 600 °C (Figure 2d). The formation of C_2F_6 and C_2F_4, small molecules, provided strong evidence of C−C cleavage and formation of perfluorocarbon radicals in thermal decomposition. The variations in products demonstrate the significant impact of temperatures on decomposition mechanisms.

After 2 h of pyrolysis of PFBS-K and PFOS-K at 500 °C, black char residuals were found in the aluminum crucibles. Another study found black chars in the pyrolysis of octafluorocyclobutane, which were assumed to be carbon.[61] ATR-FTIR was used to analyze the products. We found that residuals (74.2% mass left) from PFBS-K pyrolysis contained undecomposed PFBS-K and some new organofluorine, whereas black char (68.6% mass left) from PFOS-K contained K_2SO_4 (Figure S8). The residual products were also dissolved in methanol, diluted with water, and analyzed by UHPLC-HRMS. Undecomposed PFBS and PFOS were found in residuals at 500 °C, showing that 2 h at this temperature are insufficient to completely destroy PFSA potassium salts. $KFSO_3$ was detected in the pyrolysis of both PFBS-K and PFOS-K at 500 °C (Figure S9). FSO_3^- could be a common product, along with the formation of perfluoro-1-alkene in the pyrolysis of PFSA salts by reaction 1. When the two compounds (5−7 mg) were pyrolyzed at 600 °C for 1 h, less than 1 mg white residuals were found in aluminum crucibles. Undecomposed PFOS and PFBS were detected again from residuals by UHPLC-HRMS. FSO_3^- was detected only in the residuals of PFOS-K but not in PFBS-K at 600 °C.

$$F(CF_2)_nSO_3K \rightarrow F(CF_2)_{n-2}CF{=}CF_2 + KFSO_3 \quad (1)$$

3.2. Pyrolysis of PFBS- or PFOS-Laden GAC Samples.

3.2.1. Simultaneous Thermal Analysis and Gaseous Products in Ramp Heating. To understand the role of GAC in the thermal decomposition of PFBS and PFOS on spent GAC samples, we prepared ~30 mg of GAC equilibrated with either PFBS or PFOS for STA-MS/FTIR analysis. The TGA/DSC curves and gaseous products are shown in Figure 3. Based

https://doi.org/10.1021/acs.est.4c06805
Environ. Sci. Technol. 2024, 58, 21850−21860

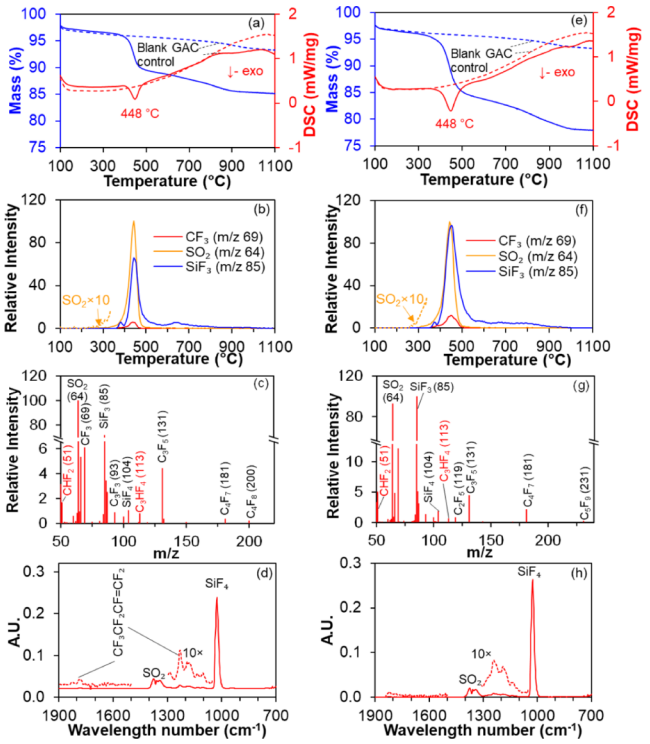

Figure 3. STA-MS/IR of GAC laden with PFBS (a-d) or PFOS (e-h). (a) and (e) TGA/DSC curve (dashed lines represent blank GAC); (b,f) formation trends of selected gaseous products represented by EI fragments; (c,g) mass spectrum of gaseous products at 448 °C (EI, 70 eV); and (d,h) FTIR spectrum (resolution, 4 cm^{-1}) of gaseous products at 448 °C for GAC laden with PFBS and PFOS, respectively. More mass spectra and FTIR spectra at different temperatures can be found in Figures S10–11. The gaseous products of blank GAC pyrolysis can be found in Figure S12.

on the TGA curves of PFBS or PFOS-laden GAC samples, the first stage of mass loss related to PFSAs is between 280 °C (the temperature of SO_2 being detected) and 470 °C, becoming faster after 400 °C with an exothermic DSC peak at 448 °C (Figure 3a and e). From 280 to 470 °C, the mass losses were 6.59% and 9.59% for PFBS- and PFOS-laden GAC, which is consistent with the preadsorbed PFBS (6.34%) and PFOS (11.76%) mass concentration, respectively. Evolved gaseous products include SO_2, SiF_4, CO_2, CO, and minor organofluorine compounds (represented by CF_3^+ m/z 69) (Figure 3c, d, g, and h). Two EI fragments, m/z 51 and m/z 113 (Figure 3c, g), can be assigned to CHF_2^+ and $C_3HF_4^+$, implying that hydrogenation may occur during the pyrolysis of PFBS- or PFOS-laden GAC. Notably, CHF_2^+ was also reported as a gaseous product when PFOS was thermally treated with a sludge matrix.[65] The second stage of mass loss occurred between 470 and 900 °C (85.62% remaining for PFBS-laden GAC and 79.45% for PFOS-laden GAC), with significant release of SiF_4. When compared to pure PFSA-K, the second stage is much longer for GAC samples, suggesting GAC may retain or adsorb fluorine products produced in the first decomposition stage. In contrast to pure PFSA potassium salt standards, the TGA/DSC curves and major decomposition products (i.e., olefins, SiF_4, and SO_2) for PFBS- or PFOS-laden GAC samples are similar, which suggests that the effects of perfluorocarbon chain length to the thermal behaviors of PFSAs are less pronounced when PFSAs are adsorbed onto GAC.

The release of SO_2 indicates that PFBS and PFOS start to decompose at temperatures as low as 280 °C when being adsorbed onto GAC. Two new signals, m/z 81 (possibly $HO-SO_2^+$) and m/z 96 (possibly SO_4^+), were also detected in the initial decomposition stage of both PFBS- and PFOS-laden GAC (Figure S12). How m/z 81 and m/z 96 were formed is not clear but could be related to the initialization of PFSA decomposition. The signals of m/z 81 and m/z 96 attained a peak at 363 °C, and their FTIR spectra are presented in Figures S10 and S11. m/z 81 and m/z 96 were not detected in STA-MS/FTIR of blank GAC, while low levels of SO_2 were observed above 350 °C (Figure S13).

3.2.2. Product Analysis at 500 and 600 °C (Isothermal Conditions). The temperatures for the pyrolysis of PFSA-laden GAC were set to 500 or 600 °C to be consistent with conditions for pure standards, allowing us to examine the effects of GAC by comparing their decomposition products. When PFBS or PFOS was preadsorbed onto GAC and pyrolyzed at 500 or 600 °C, considerable amounts of SO_2 were produced, and a large amount of organofluorine was converted into SiF_4 (Figure 4). 1-C_4F_8 and 2-C_4F_8, C_2F_4, SO_2, and SiF_4,

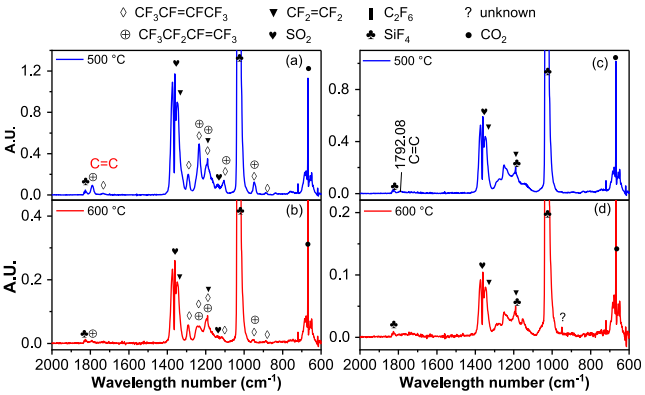

Figure 4. FTIR spectra (resolution, 2 cm^{-1}) of gaseous products in the pyrolysis of GAC laden with (a) PFBS at 500 °C, (b) PFBS at 600 °C, (c) PFOS at 500 °C, and (d) PFOS at 600 °C. Subtracted spectra from features attributable to SiF_4, SO_2, and C_2F_4 (CF_2═CF_2) can be found in Figures S14 and S15.

detected in the pyrolysis of pure PFBS-K, were also found in the pyrolysis of PFBS-laden GAC (Figure S14). 1-C_4F_8 underwent a transformation to 2-C_4F_8 when heated to 600 °C (Figure 4b), which is demonstrated by the FTIR spectrum of 1-C_4F_8 (Figure S16) obtained by subtracting the gaseous products at 600 °C from those at 500 °C. This clearly indicated that the difference of gaseous products in the pyrolysis of PFBS-laden GAC at 600 °C versus 500 °C is 1-C_4F_8. The VOF products except C_2F_4 of PFOS-laden GAC could not be identified based on FTIR spectrum (Figure 4c), only a C═C bond was found at 500 °C.

Temperatures have less influence on the decomposition products when PFOS and PFBS are adsorbed into GAC. Based on FTIR spectra, the distribution of gaseous products was more different in pyrolysis of pure PFBS/PFOS-K (Figure 2) than PFBS/PFOS-laden GAC (Figure 4) between 500 and 600 °C. For example, more C_2F_4 was produced at 500 °C than 600 °C in the pyrolysis of PFBS-K, and C_2F_6 was detected at 600 °C but was not detected at 500 °C. These differences were not observed in the pyrolysis of PFBS/PFOS-laden GAC. One possible reason is that GAC altered the decomposition

https://doi.org/10.1021/acs.est.4c06805
Environ. Sci. Technol. 2024, 58, 21850−21860

mechanisms when PFBS or PFOS are adsorbed onto the GAC surface. Another reason could be because crystal structures of salt can influence the decomposition pathways.

After PFBS- or PFOS-laden GAC were pyrolyzed for 1 h at 500 or 600 °C, the GAC was extracted by ammonium acetate (NH_4Ac) methanol solution (S2) but no PFBS/PFOS or FSO_3^- was detected by UHPLC-HRMS, which is consistent with the fact that GAC can alter and facilitate decomposition of PFSAs.

3.3. Influence of GAC on Fluorine Conversion to SiF_4. When we compared the thermal decomposition products of pure PFBS/PFOS standards and PFBS/PFOS-laden GAC samples (Table 1), we noticed clear differences in the distribution of the products, particularly in the formation of SiF_4. The presence of GAC resulted in a decrease in the temperature required for SiF_4 formation from 500 (Figure 1) to 350 °C (Figure 3) during the STA-MS/FTIR analysis. One potential explanation is that GAC contains silicon to facilitate the conversion of PFSAs into SiF_4.

To investigate the role of GAC in the formation of SiF_4, PFOS-K and fresh GAC were externally mixed (rather than adsorption) in a ceramic boat and ramp heated in a ceramic tube furnace from 100 to 900 °C at a rate of 10 °C/min in the N_2 atmosphere. A ceramic tube was used to exclude silicon interference from the reactor materials. FTIR was used to monitor gaseous products in real time, and the resulting spectra are displayed in Figure S17. The gaseous decomposition products (e.g., SO_2 and VOF) were detected around 475 °C, and then SiF_4 was formed at around 525 °C, which is consistent with the phenomena of pure PFOS-K pyrolysis in STA-MS/FTIR analysis (Figure 1f). The intensity of SiF_4 signal became much higher than VOF from ∼525 to 900 °C, which is similar to the pyrolysis of PFOS-laden GAC in STA-MS/FTIR analysis (Figure 3f). The pyrolysis of mixture and PFOS-K confirms the finding that GAC can influence the distribution of products in pyrolysis of PFSAs. During the ramp heating of the PFOS-K/GAC mixture, PFOS-K first decomposed into VOF including perfluorinated olefins, and then parts of gaseous products were released. Subsequently, some perfluorinated olefins could undergo reactions with quartz on the GAC surface to form SiF_4, which is consistent with the phenomenon discussed in Section 3.2. An additional experiment was conducted using a stainless-steel 316 tube at 500 °C, and SiF_4 was detected again by FTIR, demonstrating the GAC-mediated surface interactions for SiF_4 formation.

SEM-EDS analysis revealed that F400 GAC contains elements O, Al, Si, S, K, Ca, and Ti, in addition to C (Figure 5). Based on the safety data sheet (SDS) of F400 GAC, F400 contains quartz, titanium dioxide, aluminum oxide, calcium sulfate, and cobalt. These compounds onto GAC could potentially act as catalysts for the decomposition[66] or facilitate the conversion of PFSAs into inorganic fluorine such as SiF_4. Sasi and Xiao et al. found that nonactivated charcoals/biochars did not accelerate thermal decomposition of PFASs, indicating that insignificant role of π electron-rich, polyaromatic effects of carbon on pyrolysis of PFASs.[33] The detailed mechanisms contributing to the promotion of PFSA breakdown remain unclear. However, our study confirms that quartz facilitates the mineralization of PFSAs by generating SiF_4.

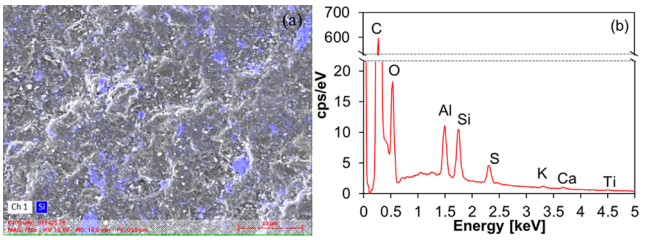

Figure 5. (a) SEM images of Si mapping of F400 GAC, and (b) Elemental analysis of clean F400 GAC surface by SEM-EDS.

In the ramp heating of mixture of PFOS-K and GAC, SO_2F_2 was found above 600 °C, and CF_4 and C_2F_6 were found above 800 °C (Figure S17). These two recalcitrant gaseous products[67−69] appear to be prevalent at high temperatures (>700 °C) in pyrolysis, which was also observed in the pyrolysis of perfluorocarboxylic acids at 780 °C.[49]

3.4. Comparative Analysis and Decomposition Mechanisms. *3.4.1. Comparisons of Thermal Stabilities and Behaviors.* While thermal stabilities of pure PFSAs have been previously reported,[33,34,70] we found that thermal stabilities and behaviors of PFSAs vary under different conditions. The similarities and differences of PFSAs under different conditions are summarized in Table 1. PFBS-K and PFOS-K were stable below 380 and 300 °C for pure standards, respectively. However, when they were adsorbed onto GAC, thermal decomposition and the release of SO_2 occurred at temperatures as low as 280 °C for both of them. These observations highlight the significance of co-occurring materials in modifying the thermal degradation of PFSAs, which needs to be considered when thermally treating PFAS-contaminated wastes.

Heating methods can influence the thermal behavior of the pure PFSA salts. During the ramp heating, both PFBS-K and PFOS-K lost more than 60% mass before reaching 500 °C in less than 50 min (Figure 1), but PFBS-K and PFOS-K only lost 25.7% and 41.4% mass in a constant heating process at 500 °C in 2 h, respectively. Faster mass loss in ramp heating could be because PFSAs-K are a solid−solid phase change materials that can change its crystalline structure from one lattice configuration to another as temperature increases, generating higher-energy structures,[71] as supported by endothermic peaks in the DSC curve without mass change (Figure 1). Higher-energy structures are easier to decompose, resulting in a faster mass loss in ramp heating.

Vaporization is common in thermal treatment. However, it is more probable for deprotonated PFBS and PFOS to undergo decomposition rather than vaporization. This is due to the low pK_a (<2) values of PFSAs,[42] indicating that PFSAs exist in an ionized form in the environmental matrices. Protonated PFBS-H and PFOS-H have a higher propensity to undergo vaporization and a transition into the gas phase. During the ramp heating, these two neutral compounds evaporated before reaching a temperature of 201 °C (Figure S18), considering PFSAs-H are thermally stable below 200 °C.,[32−34,34−40,72]

3.4.2. Decomposition Mechanisms. To gain a better understanding of potential thermal decomposition mechanisms, we performed DFT- and TST-based quantum chemical calculations to evaluate the potential surface energies for the unimolecular thermal decomposition of PFSA-K (PFBS-K shown in Figure 6a as an example and PFOS decomposition shown in Figure S19). As shown in Figure 6b, we proposed three decomposition pathways for the PFSA potassium salt ($F(CF_2)_n-SO_3K$) based on computationally derived mechanisms and the identified thermal decomposition products

https://doi.org/10.1021/acs.est.4c06805
Environ. Sci. Technol. 2024, 58, 21850−21860

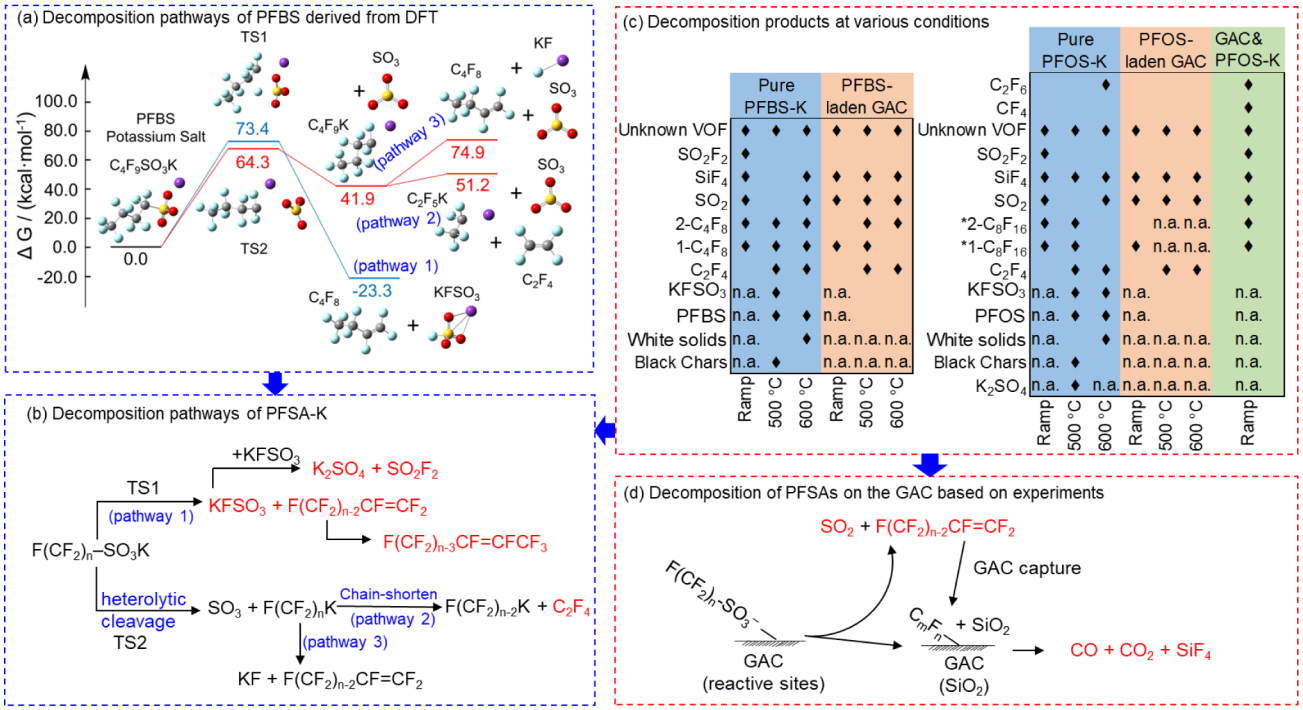

Figure 6. (a) Calculated Gibbs free energy barriers of thermal degradation of PFBS potassium salt at 800 K as an example, (b) unimolecular decomposition mechanisms of deprotonated PFSAs derived from both DFT calculations and experimental results, (c) decomposition products of PFBS/PFOS in various conditions, and (d) the decomposition of PFSAs on the surface of GAC (derived from experimental results). Final products identified by experiments (n = 4, 8) are highlighted by red texts. SeeS4.

(Figure 6c). The first pathway is an exothermic elimination reaction by the transition state (TS1) to yield perfluoro-1-alkene ($F(CF_2)_{n-2}CF=CF_2$) and $KFSO_3$ (pathway 1). The exothermic reaction is also supported by the experimental results, in which the formation of $CF_3CF_2CF=CF_2$ along with a DSC exothermic peak was found in pyrolysis PFBS-K. $F(CF_2)_{n-2}CF=CF_2$ is not thermally stable and can be converted into perfluoro-2-alkene ($F(CF_2)_{n-3}CF=CFCF_3$) (Figure S20). Residual $KFSO_3$ can be thermally decomposed into K_2SO_4 and SO_2F_2,[73] which are further demonstrated by the experimental detection (Figure 6c). Another competing channel is the dissociation of the C−S bond, which is a heterolytic cleavage via a variational transition state (TS2) (Figure 6), resulting in $F(CF_2)_nK$ and SO_3. $F(CF_2)_nK$ can be shortened by pathway 2 (C−C cleavage) with the release of $CF_2=CF_2$, a product detected in the pyrolysis of both PFBS and PFOS. Decomposition of $F(CF_2)_nK$ by pathway 3 (C−F cleavage) is another channel to yield $F(CF_2)_{n-2}CF=CF_2$(Figure 6a).

The calculated decomposition of $C_nF_{2n+1}SO_3K$ is consistent with experimental results of $C_nF_{2n+1}SO_3K$. We further calculated the decomposition of $C_4F_9SO_3^-$ (Figure S21), and the results are similar to those of $C_4F_9SO_3K$, demonstrating that K^+ minorly influences the decomposition mechanisms. However, some other counterions (e.g., NH_4^+, Al_3^+ and transition metals) could significantly change the decomposition mechanisms.[74,75] Notably, the influence of morphology or crystal structures that could change the decomposition kinetics and mechanisms as documented[76] is not considered in the simulation. The three proposed decomposition pathways did not exclude other mechanisms, as indicated by some unknown products identified in the experiments (Figure 6c).

When PFSAs are adsorbed onto GAC, the interactions between GAC (or its functionalized surface) and PFSAs can alter the thermal decomposition pathways to form SO_2 and SiF_4 even at low temperatures (<400 °C). Based on the observed products, we proposed that GAC can enhance the thermal decomposition of adsorbed PFSAs through chemical interactions between active sites or compounds on the GAC surface and PFSAs (Figure 6d), which can (1) facilitate the breakdown of the C−S bond, resulting in the degradation of the sulfonate group into SO_2, and (2) mediate surface reactions with SiO_2 to form SiF_4.

3.5. Implications. This study provides critical environmental implications for thermal treatment of PFAS. First, the lowest temperatures (e.g., 280 °C) and the most effective temperature ranges (e.g., 389−470 °C) were determined for PFSA-laden GAC decomposition in thermal regeneration of spent GAC, which is meaningful for optimization of operation parameters.[29,35,35] Second, the form of PFAS molecules (e.g., $C_nF_{2n+1}SO_3^-$ vs $C_nF_{2n+1}SO_3H$) and environmental matrix (e.g., GAC) can significantly influence and even alter the decomposition mechanisms and products. The change in mechanisms from unimolecular decomposition in pure PFAS standards to surface-mediated reactions in PFAS-laden GAC underscores the complex nature of PFAS in thermal treatment processes. We strongly suggest that the influence of environmental matrices/conditions (e.g., pH, co-occurring materials) should be considered for future research about thermal treatment of PFAS. Third, we identified some important products such as SiF_4, SO_2F_2, SO_2, $KFSO_3$, K_2SO_4, and a few olefins based on IR and MS technologies, but some VOF products remain unknown due to instrument limitations in our analysis. Gas chromatography/mass spectrometry (GC/MS) could be used to measure these unknown VOF after

https://doi.org/10.1021/acs.est.4c06805
Environ. Sci. Technol. 2024, 58, 21850−21860

separation. Finally, we found some materials, such as quartz, that can promote the mineralization of PFASs into SiF_4, which is meaningful for catalyst development.

Pyrolysis is an effective remediation strategy for PFAS-impacted materials such as GAC, soil, and biosolids,[77−81] but closing fluorine mass balance is still a challenge in thermal treatment due to unknown fluorine products.[36,37] This study revealed fluorine products, such as VOF, SiF_4, SO_2F_2, and $KFSO_3$, which contribute to the goal of closing the F mass balance. The VOF has high global warming potential and perfluoroalkenes can be oxidized into PFCAs in the atmosphere, which impose significant environmental risks.,[46,82,83] Thus, the study about detailed characterization of evolved VOF in pyrolysis of PFASs is warranted for further combustion treatment as a strategy for VOF control.,[32,67,84]

■ ASSOCIATED CONTENT

Supporting Information

The Supporting Information is available free of charge at https://pubs.acs.org/doi/10.1021/acs.est.4c06805.

Preparation of PFAS-laden GAC samples, chemical information, qualitative analysis method, diagrams of thermal analyzers and tube furnace, mass spectra, FTIR spectra, formation trends of EI fragments of gaseous products, detection of FSO_3^-, TGA/DSC curves, theoretical potential energy profiles (PDF)

■ AUTHOR INFORMATION

Corresponding Author

Ying-Hsuan Lin − *Department of Environmental Sciences and Environmental Toxicology Graduate Program, University of California, Riverside, California 92521, United States;* orcid.org/0000-0001-8904-1287; Email: ying-hsuan.lin@ucr.edu

Authors

Junli Wang − *Department of Environmental Sciences, University of California, Riverside, California 92521, United States;* orcid.org/0000-0001-8716-0338

Kunpeng Chen − *Department of Environmental Sciences, University of California, Riverside, California 92521, United States;* orcid.org/0000-0002-9430-9257

Bosen Jin − *Department of Chemical and Environmental Engineering, University of California, Riverside, California 92521, United States;* orcid.org/0000-0001-7659-3437

Wonsik Woo − *Environmental Toxicology Graduate Program, University of California, Riverside, California 92521, United States;* orcid.org/0009-0003-3588-2744

Michael Lum − *Department of Environmental Sciences, University of California, Riverside, California 92521, United States;* orcid.org/0000-0001-5829-5452

Alexa Canchola − *Environmental Toxicology Graduate Program, University of California, Riverside, California 92521, United States;* orcid.org/0000-0001-8285-4795

Yiwen Zhu − *Department of Chemical and Environmental Engineering, University of California, Riverside, California 92521, United States*

Yujie Men − *Department of Chemical and Environmental Engineering, University of California, Riverside, California 92521, United States;* orcid.org/0000-0001-9811-3828

Jinyong Liu − *Department of Chemical and Environmental Engineering, University of California, Riverside, California 92521, United States;* orcid.org/0000-0003-1473-5377

Complete contact information is available at: https://pubs.acs.org/10.1021/acs.est.4c06805

Notes

The authors declare no competing financial interest.

■ ACKNOWLEDGMENTS

This research was supported by the DoD Strategic Environmental Research and Development Program (Project ER21-1191) and the UCR OASIS Internal Funding Award. M.L. was supported by an NSF graduate research fellowship. W.W. and A.C. were supported in part by an NRSA T32 training grant (T32ES018827). We greatly appreciate Dr. Brett Boote's assistance in the simultaneous thermal analysis at Iowa State University. Computations were performed using the computer clusters and data storage resources of the High-Performance Computer Cluster at the University of California, Riverside, which were funded by grants from the National Science Foundation (MRI-2215705 and MRI-1429826) and the National Institutes of Health (1S10OD016290-01A1).

■ REFERENCES

(1) Johnson, G. R.; Brusseau, M. L.; Carroll, K. C.; Tick, G. R.; Duncan, C. M. Global distributions, source-type dependencies, and concentration ranges of per- and polyfluoroalkyl substances in groundwater. *Sci. Total Environ.* **2022**, *841*, 156602.

(2) Pfotenhauer, D.; Sellers, E.; Olson, M.; Praedel, K.; Shafer, M. PFAS concentrations and deposition in precipitation: An intensive 5-month study at National Atmospheric Deposition Program − National trends sites (NADP-NTN) across Wisconsin, USA. *Atmos. Environ.* **2022**, *291*, 119368.

(3) Chen, H.; Zhang, L.; Li, M.; Yao, Y.; Zhao, Z.; Munoz, G.; Sun, H. Per- and polyfluoroalkyl substances (PFASs) in precipitation from mainland China: Contributions of unknown precursors and short-chain (C2C3) perfluoroalkyl carboxylic acids. *Water Res.* **2019**, *153*, 169−177.

(4) Cousins, I. T.; Johansson, J. H.; Salter, M. E.; Sha, B.; Scheringer, M. Outside the Safe Operating Space of a New Planetary Boundary for Per- and Polyfluoroalkyl Substances (PFAS). *Environ. Sci. Technol.* **2022**, *56* (16), 11172−11179.

(5) McDonough, C. A.; Choyke, S.; Ferguson, P. L.; DeWitt, J. C.; Higgins, C. P. Bioaccumulation of Novel Per- and Polyfluoroalkyl Substances in Mice Dosed with an Aqueous Film-Forming Foam. *Environ. Sci. Technol.* **2020**, *54* (9), 5700−5709.

(6) Ghisi, R.; Vamerali, T.; Manzetti, S. Accumulation of perfluorinated alkyl substances (PFAS) in agricultural plants: A review. *Environ. Res.* **2019**, *169*, 326−341.

(7) Pérez, F.; Nadal, M.; Navarro-Ortega, A.; Fàbrega, F.; Domingo, J. L.; Barceló, D.; Farré, M. Accumulation of perfluoroalkyl substances in human tissues. *Environ. Int.* **2013**, *59*, 354−362.

(8) Wen, Y.; Mirji, N.; Irudayaraj, J. Epigenetic toxicity of PFOA and GenX in HepG2 cells and their roles in lipid metabolism. *Toxicol. In Vitro* **2020**, *65*, 104797.

(9) Sznajder-Katarzyńska, K.; Surma, M.; Cieślik, I. A Review of Perfluoroalkyl Acids (PFAAs) in terms of sources, applications, human exposure, dietary intake, toxicity, legal regulation, and methods of determination. *J. Chem.* **2019**, *2019*, 2717528.

(10) Barisci, S.; Suri, R. Occurrence and removal of poly/perfluoroalkyl substances (PFAS) in municipal and industrial wastewater treatment plants. *Water Sci. Technol.* **2021**, *84* (12), 3442−3468.

(11) Appleman, T. D.; Higgins, C. P.; Quiñones, O.; Vanderford, B. J.; Kolstad, C.; Zeigler-Holady, J. C.; Dickenson, E. R. V. Treatment

of poly- and perfluoroalkyl substances in U.S. full-scale water treatment systems. *Water Res.* **2014**, *51*, 246−255.
(12) Rao, U.; Su, Y.; Khor, C. M.; Jung, B.; Ma, S.; Cwiertny, D. M.; Wong, B. M.; Jassby, D. Structural Dependence of Reductive Defluorination of Linear PFAS Compounds in a UV/Electrochemical System. *Environ. Sci. Technol.* **2020**, *54* (17), 10668−10677.
(13) Zweigle, J.; Bugsel, B.; Schmitt, M.; Zwiener, C. Electrochemical Oxidation of 6: 2 Polyfluoroalkyl Phosphate Diester—Simulation of Transformation Pathways and Reaction Kinetics with Hydroxyl Radicals. *Environ. Sci. Technol.* **2021**, *55* (16), 11070−11079.
(14) Liu, Z.; Chen, Z.; Gao, J.; Yu, Y.; Men, Y.; Gu, C.; Liu, J. Accelerated Degradation of Perfluorosulfonates and Perfluorocarboxylates by UV/Sulfite + Iodide: Reaction Mechanisms and System Efficiencies. *Environ. Sci. Technol.* **2022**, *56* (6), 3699−3709.
(15) Abusallout, I.; Wang, J.; Hanigan, D. Emerging investigator series: rapid defluorination of 22 per- and polyfluoroalkyl substances in water using sulfite irradiated by medium-pressure UV. *Environ. Sci.: Water Res. Technol.* **2021**, *7* (9), 1552−1562.
(16) Tenorio, R.; Liu, J.; Xiao, X.; Maizel, A. C.; Higgins, C. P.; Schaefer, C. E.; Strathmann, T. J. Destruction of per- and polyfluoroalkyl substances (PFASs) in aqueous film-forming foam (AFFF) with UV-sulfite photo-reductive treatment. *Environ. Sci. Technol.* **2020**, *54* (11), 6957−6967.
(17) Bentel, M. J.; Liu, Z.; Yu, Y.; Gao, J.; Men, Y.; Liu, J. Enhanced Degradation of Perfluorocarboxylic Acids (PFCAs) by UV/Sulfite Treatment: Reaction Mechanisms and System Efficiencies at pH 12. *Environ. Sci. Technol. Lett.* **2020**, *7* (5), 351−357.
(18) Liu, Z.; Bentel, M. J.; Yu, Y.; Ren, C.; Gao, J.; Pulikkal, V. F.; Sun, M.; Men, Y.; Liu, J. Near-Quantitative Defluorination of Perfluorinated and Fluorotelomer Carboxylates and Sulfonates with Integrated Oxidation and Reduction. *Environ. Sci. Technol.* **2021**, *55* (10), 7052−7062.
(19) Nau-Hix, C.; Multari, N.; Singh, R. K.; Richardson, S.; Kulkarni, P.; Anderson, R. H.; Holsen, T. M.; Mededovic Thagard, S. Field Demonstration of a Pilot-Scale Plasma Reactor for the Rapid Removal of Poly- and Perfluoroalkyl Substances in Groundwater. *ACS ES&T Water* **2021**, *1* (3), 680−687.
(20) Singh, R. K.; Fernando, S.; Baygi, S. F.; Multari, N.; Thagard, S. M.; Holsen, T. M. Breakdown Products from Perfluorinated Alkyl Substances (PFAS) Degradation in a Plasma-Based Water Treatment Process. *Environ. Sci. Technol.* **2019**, *53* (5), 2731−2738.
(21) Stratton, G. R.; Dai, F.; Bellona, C. L.; Holsen, T. M.; Dickenson, E. R. V.; Mededovic Thagard, S. Plasma-Based Water Treatment: Efficient Transformation of Perfluoroalkyl Substances in Prepared Solutions and Contaminated Groundwater. *Environ. Sci. Technol.* **2017**, *51* (3), 1643−1648.
(22) Cui, J.; Gao, P.; Deng, Y. Destruction of Per- and Polyfluoroalkyl Substances (PFAS) with Advanced Reduction Processes (ARPs): A Critical Review. *Environ. Sci. Technol.* **2020**, *54* (7), 3752−3766.
(23) Nzeribe, B. N.; Crimi, M.; Mededovic Thagard, S.; Holsen, T. M. Physico-Chemical Processes for the Treatment of Per-And Polyfluoroalkyl Substances (PFAS): A review. *Crit. Rev. Environ. Sci. Technol.* **2019**, *49* (10), 866−915.
(24) Eun, H.; Shimamura, K.; Asano, T.; Yamazaki, E.; Taniyasu, S.; Yamashita, N. Removal of perfluoroalkyl substances from water by activated carbons: Adsorption of perfluorooctane sulfonate and perfluorooctanoic acid. *Environ. Monit. Contam. Res.* **2022**, *2*, 88−93.
(25) Chow, S. J.; Croll, H. C.; Ojeda, N.; Klamerus, J.; Capelle, R.; Oppenheimer, J.; Jacangelo, J. G.; Schwab, K. J.; Prasse, C. Comparative investigation of PFAS adsorption onto activated carbon and anion exchange resins during long-term operation of a pilot treatment plant. *Water Res.* **2022**, *226*, 119198.
(26) Rodowa, A. E.; Knappe, D. R. U.; Chiang, S.-Y. D.; Pohlmann, D.; Varley, C.; Bodour, A.; Field, J. A. Pilot scale removal of per- and polyfluoroalkyl substances and precursors from AFFF-impacted groundwater by granular activated carbon. *Environ. Sci.: Water Res. Technol.* **2020**, *6* (4), 1083−1094.
(27) Sonmez Baghirzade, B.; Zhang, Y.; Reuther, J. F.; Saleh, N. B.; Venkatesan, A. K.; Apul, O. G. Thermal Regeneration of Spent Granular Activated Carbon Presents an Opportunity to Break the Forever PFAS Cycle. *Environ. Sci. Technol.* **2021**, *55* (9), 5608−5619.
(28) Helmer, R. W.; Reeves, D. M.; Cassidy, D. P. Per- and Polyfluorinated Alkyl Substances (PFAS) cycling within Michigan: Contaminated sites, landfills and wastewater treatment plants. *Water Res.* **2022**, *210*, 117983.
(29) DiStefano, R.; Feliciano, T.; Mimna, R. A.; Redding, A. M.; Matthis, J. Thermal destruction of PFAS during full-scale reactivation of PFAS-laden granular activated carbon. *Remediation J.* **2022**, *32*, 231−238.
(30) Matthis, J.; Carr, S. Reactivation of Spent Activated Carbon Used for PFAS Adsorption. In *Perfluoroalkyl Substances in the Environment*; CRC Press, 2018, pp. 303−324.
(31) Moore, B. C.; Cannon, F. S.; Metz, D. H.; Demarco, J. GAC pore structure in Cincinnati during full-scale treatment/reactivation. *J. - Am. Water Works Assoc.* **2003**, *95* (2), 103−112.
(32) Wang, J.; Lin, Z.; He, X.; Song, M.; Westerhoff, P.; Doudrick, K.; Hanigan, D. Critical Review of Thermal Decomposition of Per- and Polyfluoroalkyl Substances: Mechanisms and Implications for Thermal Treatment Processes. *Environ. Sci. Technol.* **2022**, *56* (9), 5355−5370.
(33) Sasi, P. C.; Alinezhad, A.; Yao, B.; Kubátová, A.; Golovko, S. A.; Golovko, M. Y.; Xiao, F. Effect of Granular Activated Carbon and Other Porous Materials on Thermal Decomposition of Per- and Polyfluoroalkyl Substances: Mechanisms and Implications for Water Purification. *Water Res.* **2021**, *200*, 117271.
(34) Xiao, F.; Sasi, P. C.; Yao, B.; Kubátová, A.; Golovko, S. A.; Golovko, M. Y.; Soli, D. Thermal Stability and Decomposition of Perfluoroalkyl Substances on Spent Granular Activated Carbon. *Environ. Sci. Technol. Lett.* **2020**, *7* (5), 343−350.
(35) San Miguel, G.; Lambert, S. D.; Graham, N. J. D. The regeneration of field-spent granular-activated carbons. *Water Res.* **2001**, *35* (11), 2740−2748.
(36) Watanabe, N.; Takemine, S.; Yamamoto, K.; Haga, Y.; Takata, M. Residual organic fluorinated compounds from thermal treatment of PFOA, PFHxA and PFOS adsorbed onto granular activated carbon (GAC). *J. Mater. Cycles Waste Manage.* **2016**, *18* (4), 625−630.
(37) Watanabe, N.; Takata, M.; Takemine, S.; Yamamoto, K. Thermal mineralization behavior of PFOA, PFHxA, and PFOS during reactivation of granular activated carbon (GAC) in nitrogen atmosphere. *Environ. Sci. Pollut. Res.* **2018**, *25* (8), 7200−7205.
(38) Weber, N. H.; Delva, C. S.; Stockenhuber, S. P.; Grimison, C. C.; Lucas, J. A.; Mackie, J. C.; Stockenhuber, M.; Kennedy, E. M. Thermal Mineralization of Perfluorooctanesulfonic Acid (PFOS) to HF, CO2, and SO2. *Ind. Eng. Chem. Res.* **2023**, *62* (2), 881−892.
(39) Weber, N. H.; Delva, C. S.; Stockenhuber, S. P.; Grimison, C. C.; Lucas, J. A.; Mackie, J. C.; Stockenhuber, M.; Kennedy, E. M. Thermal Decomposition of Perfluorooctanesulfonic Acid (PFOS) in the Presence of Water Vapor. *Ind. Eng. Chem. Res.* **2022**, *61* (41), 15146−15155.
(40) Weber, N. H.; Delva, C. S.; Stockenhuber, S. P.; Grimison, C. C.; Lucas, J. A.; Mackie, J. C.; Stockenhuber, M.; Kennedy, E. M. Modeling and Experimental Study on the Thermal Decomposition of Perfluorooctanesulfonic Acid (PFOS) in an α-Alumina Reactor. *Ind. Eng. Chem. Res.* **2022**, *61* (16), 5453−5463.
(41) Khan, M. Y.; So, S.; da Silva, G. Decomposition kinetics of perfluorinated sulfonic acids. *Chemosphere* **2020**, *238*, 124615.
(42) Rayne, S.; Forest, K. Perfluoroalkyl sulfonic and carboxylic acids: A critical review of physicochemical properties, levels and patterns in waters and wastewaters, and treatment methods. *J. Environ. Sci. Health, Part A* **2009**, *44* (12), 1145−1199.
(43) Belkouteb, N.; Franke, V.; McCleaf, P.; Köhler, S.; Ahrens, L. Removal of per- and polyfluoroalkyl substances (PFASs) in a full-scale drinking water treatment plant: Long-term performance of granular activated carbon (GAC) and influence of flow-rate. *Water Res.* **2020**, *182*, 115913.

(44) Yu, Z.; Peldszus, S.; Huck, P. M. Adsorption characteristics of selected pharmaceuticals and an endocrine disrupting compound—Naproxen, carbamazepine and nonylphenol—on activated carbon. *Water Res.* **2008**, *42* (12), 2873−2882.
(45) Jaramillo, J.; Gómez-Serrano, V.; Álvarez, P. M. Enhanced adsorption of metal ions onto functionalized granular activated carbons prepared from cherry stones. *J. Hazard. Mater.* **2009**, *161* (2−3), 670−676.
(46) Young, C. J.; Hurley, M. D.; Wallington, T. J.; Mabury, S. A. Atmospheric chemistry of perfluorobutenes (CF3CFCFCF3 and CF3CF2CFCF2): Kinetics and mechanisms of reactions with OH radicals and chlorine atoms, IR spectra, global warming potentials, and oxidation to perfluorocarboxylic acids. *Atmos. Environ.* **2009**, *43* (24), 3717−3724.
(47) *NIST Chemistry WebBook, NIST Standard Reference Database Number 69*, Linstrom, P. J.; Mallard, W. G., Eds; National Institute of Standards and Technology: Gaithersburg MD, 2023. DOI: .
(48) *SpectraBase*; John Wiley & Sons, Inc., https://spectrabase.com/ . accessed 2022−March−09.
(49) Wang, J.; Song, M.; Abusallout, I.; Hanigan, D. Thermal Decomposition of Two Gaseous Perfluorocarboxylic Acids: Products and Mechanisms. *Environ. Sci. Technol.* **2023**, *57* (15), 6179−6187.
(50) Baker, T. J.; Tonkyn, R. G.; Thompson, C. J.; Dunlap, M. K.; Koster van Groos, P. G.; Thakur, N. A.; Wilhelm, M. J.; Myers, T. L.; Johnson, T. J. An infrared spectral database for gas-phase quantitation of volatile per- and polyfluoroalkyl substances (PFAS). *J. Quant. Spectrosc. Radiat. Transfer* **2023**, *295*, 108420.
(51) Jin, B.; Liu, H.; Che, S.; Gao, J.; Yu, Y.; Liu, J.; Men, Y. Substantial defluorination of polychlorofluorocarboxylic acids triggered by anaerobic microbial hydrolytic dechlorination. *Nature Water* **2023**, *1* (5), 451−461.
(52) Boese, A. D.; Martin, J. M. L. Development of density functionals for thermochemical kinetics. *J. Chem. Phys.* **2004**, *121* (8), 3405−3416.
(53) Ditchfield, R.; Hehre, W. J.; Pople, J. A. Self-Consistent Molecular-Orbital Methods. IX. An Extended Gaussian-Type Basis for Molecular-Orbital Studies of Organic Molecules. *J. Chem. Phys.* **1971**, *54* (2), 724−728.
(54) Kozuch, S.; Martin, J. M. L. DSD-PBEP86: in search of the best double-hybrid DFT with spin-component scaled MP2 and dispersion corrections. *Phys. Chem. Chem. Phys.* **2011**, *13* (45), 20104−20107.
(55) Grimme, S.; Ehrlich, S.; Goerigk, L. Effect of the damping function in dispersion corrected density functional theory. *J. Comput. Chem.* **2011**, *32* (7), 1456−1465.
(56) Weigend, F.; Ahlrichs, R. Balanced basis sets of split valence, triple zeta valence and quadruple zeta valence quality for H to Rn: Design and assessment of accuracy. *Phys. Chem. Chem. Phys.* **2005**, *7* (18), 3297−3305.
(57) Gonzalez, C.; Schlegel, H. B. An improved algorithm for reaction path following. *J. Chem. Phys.* **1989**, *90* (4), 2154−2161.
(58) Khan, M. Y.; Song, J.; Narimani, M.; da Silva, G. Thermal decomposition mechanism and kinetics of perfluorooctanoic acid (PFOA) and other perfluorinated carboxylic acids: a theoretical study. *Environ. Sci. Process Impacts* **2022**, *24* (12), 2475−2487.
(59) Weber, N. H.; Dixon, L. J.; Stockenhuber, S. P.; Grimison, C. C.; Lucas, J. A.; Mackie, J. C.; Stockenhuber, M.; Kennedy, E. M. Thermal decomposition of PFOA: Influence of reactor and reaction conditions on product formation. *Chem. Eng. Sci.* **2023**, *278*, 118924.
(60) Baasandorj, M.; Papadimitriou, V. C.; Burkholder, J. B. Rate Coefficients for the Gas-Phase Reaction of (E)- and (Z)-CF(3)CF horizontal lineCFCF(3) with the OH Radical and Cl-Atom. *J. Phys. Chem. A* **2019**, *123* (24), 5051−5060.
(61) Butler, J. N. The Thermal Decomposition of Octafluorocyclobutane. *J. Am. Chem. Soc.* **1962**, *84* (8), 1393−1398.
(62) Krusic, P. J.; Marchione, A. A.; Roe, D. C. Gas-phase NMR studies of the thermolysis of perfluorooctanoic acid. *J. Fluorine Chem.* **2005**, *126* (11), 1510−1516.
(63) Merlini, A.; Claumann, C.; Zibetti, A. W.; Coirolo, A.; Rieg, T.; Machado, R. A. F. Kinetic Study of the Thermal Decomposition of Cellulose Nanocrystals with Different Crystal Structures and Morphologies. *Ind. Eng. Chem. Res.* **2020**, *59* (30), 13428−13439.
(64) Hughey, K. D.; Gallagher, N. B.; Zhao, Y.; Thakur, N.; Bradley, A. M.; Koster van Groos, P. G.; Johnson, T. J. PFAS Remediation: Evaluating the Infrared Spectra of Complex Gaseous Mixtures to Determine the Efficacy of Thermal Decomposition of PFAS. *Chemosphere* **2024**, *362*, 142631.
(65) Wang, F.; Shih, K.; Lu, X.; Liu, C. Mineralization Behavior of Fluorine in Perfluorooctanesulfonate (PFOS) during Thermal Treatment of Lime-Conditioned Sludge. *Environ. Sci. Technol.* **2013**, *47* (6), 2621−2627.
(66) Biswas, S.; Wong, B. M. Degradation of Perfluorooctanoic Acid on Aluminum Oxide Surfaces: New Mechanisms from Ab Initio Molecular Dynamics Simulations. *Environ. Sci. Technol.* **2023**, *57* (16), 6695−6702.
(67) Krug, J. D.; Lemieux, P. M.; Lee, C. W.; Ryan, J. V.; Kariher, P. H.; Shields, E. P.; Wickersham, L. C.; Denison, M. K.; Davis, K. A.; Swensen, D. A.; Burnette, R. P.; Wendt, J. O. L.; Linak, W. P. Combustion of C1 and C2 PFAS: Kinetic modeling and experiments. *J. Air Waste Manage Assoc.* **2022**, *72* (3), 256−270.
(68) Wang, H.; Castillo, Á.; Bozzelli, J. W. Thermochemical Properties Enthalpy, Entropy, and Heat Capacity of C1−C4 Fluorinated Hydrocarbons: Fluorocarbon Group Additivity. *J. Phys. Chem. A* **2015**, *119* (29), 8202−8215.
(69) Lee, M. C.; Choi, W. Efficient Destruction of CF4 through In Situ Generation of Alkali Metals from Heated Alkali Halide Reducing Mixtures. *Environ. Sci. Technol* **2002**, *36* (6), 1367−1371.
(70) Xiao, F.; Challa Sasi, P.; Alinezhad, A.; Sun, R.; Abdulmalik Ali, M. Thermal Phase Transition and Rapid Degradation of Forever Chemicals (PFAS) in Spent Media Using Induction Heating. *ACS ES&T Eng.* **2023**, *3* (9), 1370−1380.
(71) Fallahi, A.; Guldentops, G.; Tao, M.; Granados-Focil, S.; Van Dessel, S. Review on solid-solid phase change materials for thermal energy storage: Molecular structure and thermal properties. *Appl. Therm. Eng.* **2017**, *127*, 1427−1441.
(72) Weber, N. H.; Grimison, C. C.; Lucas, J. A.; Mackie, J. C.; Stockenhuber, M.; Kennedy, E. M. Influence of reactor composition on the thermal decomposition of perfluorooctanesulfonic acid (PFOS). *J. Hazard. Mater.* **2024**, *461*, 132665.
(73) Simons, J. H. *Fluorine Chemistry*; Academic Press, New York, 1950.
(74) LaZerte, J. D.; Hals, L. J.; Reid, T. S.; Smith, G. H. Pyrolyses of the Salts of the Perfluoro Carboxylic Acids. *J. Am. Chem. Soc.* **1953**, *75* (18), 4525−4528.
(75) Blotevogel, J.; Giraud, R. J.; Rappé, A. K. Incinerability of PFOA and HFPO-DA: Mechanisms, kinetics, and thermal stability ranking. *Chem. Eng. J.* **2023**, *457*, 141235.
(76) Chen, H.; Zhang, T.; Zhang, J.; Qiao, X.; Yu, K. Crystal structure, thermal decomposition mechanism and explosive properties of [Na(H2TNPG)(H2O)2]n. *J. Hazard. Mater.* **2006**, *129* (1), 31−36.
(77) Alinezhad, A.; Challa Sasi, P.; Zhang, P.; Yao, B.; Kubátová, A.; Golovko, S. A.; Golovko, M. Y.; Xiao, F. An Investigation of Thermal Air Degradation and Pyrolysis of Per- and Polyfluoroalkyl Substances and Aqueous Film-Forming Foams in Soil. *ACS ES&T Eng.* **2022**, *2* (2), 198−209.
(78) Thoma, E. D.; Wright, R. S.; George, I.; Krause, M.; Presezzi, D.; Villa, V.; Preston, W.; Deshmukh, P.; Kauppi, P.; Zemek, P. G. Pyrolysis processing of PFAS-impacted biosolids, a pilot study. *J. Air Waste Manage. Assoc.* **2022**, *72* (4), 309−318.
(79) Thompson, J. T.; Robey, N. M.; Tolaymat, T. M.; Bowden, J. A.; Solo-Gabriele, H. M.; Townsend, T. G. Underestimation of Per- and Polyfluoroalkyl Substances in Biosolids: Precursor Transformation During Conventional Treatment. *Environ. Sci. Technol.* **2023**, *57* (9), 3825−3832.
(80) Bamdad, H.; Papari, S.; Moreside, E.; Berruti, F. High-Temperature Pyrolysis for Elimination of Per- and Polyfluoroalkyl Substances (PFAS) from Biosolids. *Processes* **2022**, *10* (11), 2187.

(81) Kundu, S.; Patel, S.; Halder, P.; Patel, T.; Hedayati Marzbali, M.; Pramanik, B. K.; Paz-Ferreiro, J.; de Figueiredo, C. C.; Bergmann, D.; Surapaneni, A.; Megharaj, M.; Shah, K. Removal of PFASs from biosolids using a semi-pilot scale pyrolysis reactor and the application of biosolids derived biochar for the removal of PFASs from contaminated water. *Environ. Sci.: Water Res. Technol.* **2021**, *7* (3), 638−649.
(82) Roehl, C.; Boglu, D.; Brühl, C.; Moortgat, G. Infrared band intensities and global warming potentials of CF4, C2F6, C3F8, C4F10, C5F12, and C6F14. *Geophys. Res. Lett.* **1995**, *22* (7), 815−818.
(83) Bravo, I.; Aranda, A.; Hurley, M. D.; Marston, G.; Nutt, D. R.; Shine, K. P.; Smith, K.; Wallington, T. J. Infrared absorption spectra, radiative efficiencies, and global warming potentials of perfluorocarbons: Comparison between experiment and theory. *J. Geophys. Res.* **2010**, *115*, D24317.
(84) Shields, E. P.; Krug, J. D.; Roberson, W. R.; Jackson, S. R.; Smeltz, M. G.; Allen, M. R.; Burnette, R. P.; Nash, J. T.; Virtaranta, L.; Preston, W.; Liberatore, H. K.; Wallace, M. A. G.; Ryan, J. V.; Kariher, P. H.; Lemieux, P. M.; Linak, W. P. Pilot-Scale Thermal Destruction of Per- and Polyfluoroalkyl Substances in a Legacy Aqueous Film Forming Foam. *ACS ES&T Eng.* **2023**, *3* (9), 1308−1317.

https://doi.org/10.1021/acs.est.4c06805
Environ. Sci. Technol. 2024, 58, 21850−21860